Eugene Wong

Project was conducted under supervision of Dr. Michele Guala and sponsored by The University of Minnesota Undergraduate Research Opportunities Program (UROP).

Direct experimental assessment of scale-dependent migration velocities in river bedforms

<u>Symbols</u>

U	Horizontal Velocity
V	Vertical Velocity
GU,GV	Globally Filtered Velocity
X,Y	Spatial Coordinates
t	Time
ρ	Auto-Correlation Sequence
τ	Scan Index
RMS	Root Mean Square
nx,ny	Interrogation Window Dimensions
$U`_{xy}$	Fluctuation from Global Averaged Velocity
$U`_{xyt}$	Fluctuation from Local Averaged Velocity
NaN	Undefined value
mm	Millimeter
s	Seconds

Introduction

Based on the article, “Spectral description of migrating bed forms and sediment transport” (Guala et al. 2014), bed forms of distinct spatial dimensions possess varying migration velocities corresponding to their size. The article demonstrates statistical behavior of larger bed form structures to migrate at a slower pace compared to those of a smaller nature. As a result, the bedform geometry resolved spatially was unable to be rigorously transformed with respect to time, and vice versa, thus proposing a suggested relationship between the bedform length and the bedform period and an improved model for bedform migration.

Following the suggested improved model offered by the article, this project aims to test the proposed functional relationship between bedform length and period:

1) Testing the viability of a space-time Fourier decomposition to predict bedform migration.

2) Testing if the following relation proposed from (Guala et al. 2014) holds under substantially different channel size and geometry. $CV\ (T) = C\sqrt{\ u{*}ds\ T}$ (1) where C is assumed to be a constant = 2, u* is the shear velocity (m/s), ds is the median sediment diameter (m), T is the mean bed form period (s) and Cv is convection velocity of bedforms (m/s).

3) Testing the reliability of the mass flux predicted via the spectral method (Fourier decomposition).

So far, Guala et al. developed a method for the estimate of convection velocities, based on the Fourier analysis, that has never been tested against direct measurements of bed surface velocity or direct measurements of sediment mass flux, simply because such measurements have never been available (here or elsewhere). Spatio-temporally resolved bathymetry measurements were however recently obtained from an experiment conducted in the SAFL main channel at unprecedented details, via Particle Image Velocimetry (PIV) applied directly on field of bed elevation. The results are represented in Figure 1 (Guala, 2015). We are going to use these direct measurements of surface velocity, applied on this new set of data, to test the working assumptions discussed in Guala et al (2014). The Fourier decomposition of bedform migration is effectively reproducing the bedform as a superposition, or sum, of many sinusoidal components each one characterized by a well-defined (spatial or temporal) scale, amplitude, and convection velocity. Each point in the contours depicted in Figure 2 (from Guala et al. 2014) represent a contribution, to the overall bed elevation variance, by a specific bedform period T and wavelength λ . Their ratio, represent a convection velocity, which can be statistically modeled using equation 1 (the straight black line in figure 2), or experimentally observed using the surface velocity in figure 1. The main point of this work is to compare these two estimates. This project aims at building and validating a method to estimate sediment discharge in rivers, by using only measurements of bed elevations in time, which are easy and affordable to implement.

Interrogation Window Selection for PIV

The interrogation window dimensions, [nx,ny], need to be suitable to accurately describe the velocity field of the channel. Decreasing the window size, or increasing resolution, will result in a better locally defined velocity field, however at the risk of increasing the resolution to the point of insufficient particles in each window, thus affecting accuracy. The default guess at set at [256,32] and nx is varied.

The number of negative U vectors will be used as a measure of the efficacy of the window size as backflow should not exist in the channel. Results below are averaged over 9 vector fields.

nx	**Percentage of negative vectors (%)**
256	0.7515
128	6.3319
64	15.9405

Table 1:Percentage of negative horizontal vectors with respect to variations in nx

At <1% negative vectors, 256 is seemingly to be the most suitable value for nx.

Ruling 64 out, further analysis on nx determines 256 to be the most suitable as follows:

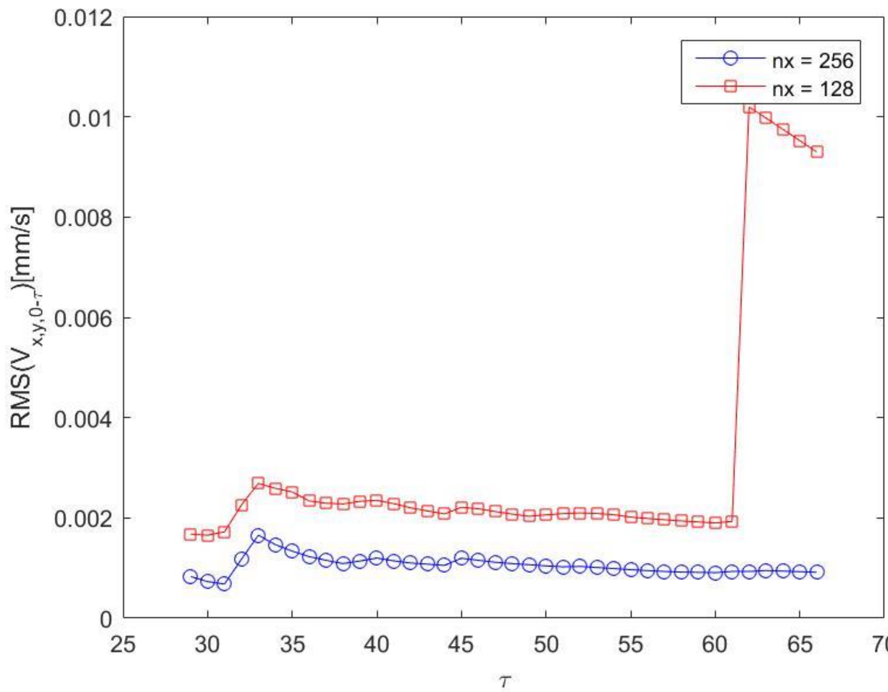

Figure 1: Convergence study of RMS velocity averaged over the entire vector field and over an increasing number of scans 0 τ

Fluctuations using the mean velocity averaged across x,y & t seem to be increased compared to local fluctuations. Overall, they display similar behavior and also possess the tendency to

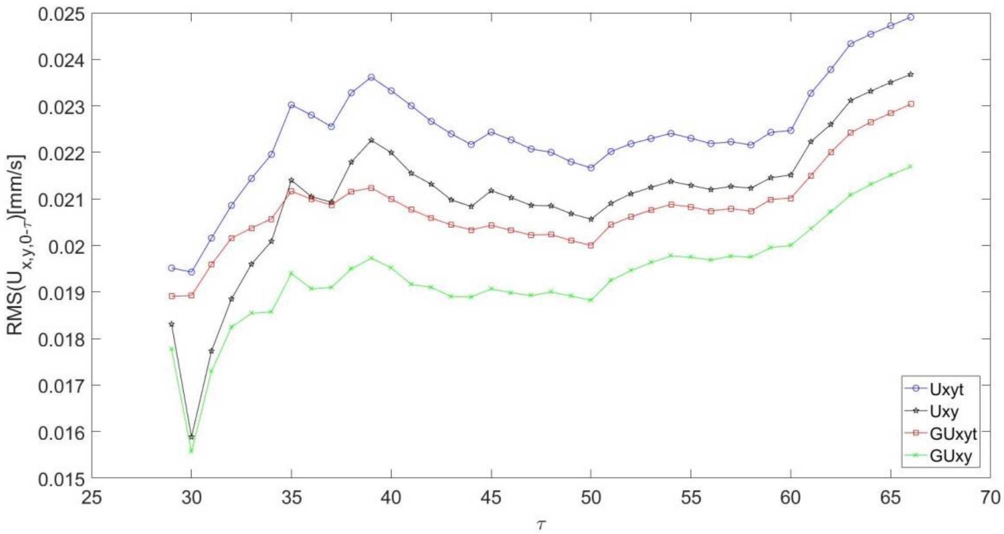

Figure 2: Comparison of convergence study of RMS velocity between the filtered (Gu, Gv) and unfiltered data; t indicates fluctuations computed using a local average, not a global (one number) average

increase with time.

RMS analysis shows a spike using the 128 window but the 256 window converges as expected. Data filtering was attempted (Gu, Gv from matpiv subroutine) to fix the RMS spike in the 128 window but results were not promising as several vectors in the globally filtered data were undefined. The filtered data held 1.26% NaNs whereas unfiltered data held 0% NaNs. Therefore, unfiltered data was opted to continue with analysis.

Following that, nx is set to 256 to proceed with ny selection.
Similarly,

Ny	**Percentage of negative vectors (%)**
64	0.3731
32	0.7515
16	1.3979

Table 2: Percentage of negative horizontal vectors with respect to variations in ny

Unlike nx, the variations in ny produced insignificant change in the percentage of negative velocity vectors. The percentage of NaNs in all the unfiltered vectors is also found to remain null.

Attempting use of mean velocity as the measure,

ny	Mean Velocity, U (mm/s)
64	0.0272
32	0.0282
16	0.0287

Table 3: Mean horizontal velocity with respect to variations in ny

The variations in ny is found to be insignificant with respect to the mean velocity.

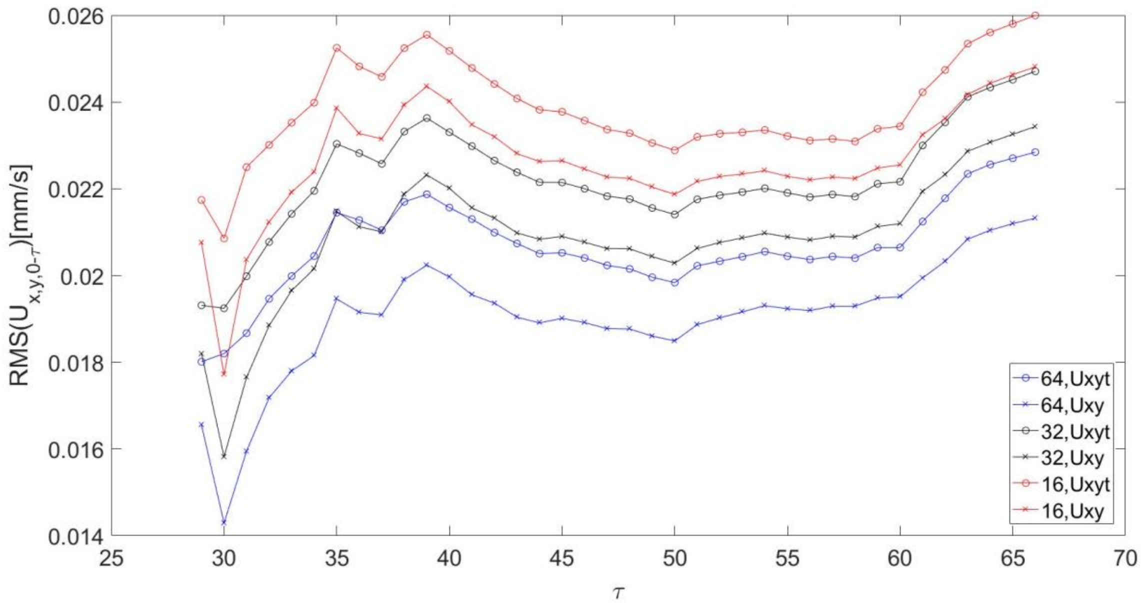

Figure 3: Comparison of convergence study of RMS velocity between variations in ny; t indicates fluctuations computed using a local average, not a global (one number) average

The behavior of the RMS plots is consistent regardless of the window size. Following that, ny seems to have minimal effect on the results of analysis, therefore 32 is chosen to be set as ny, proceeding with further analysis using the default **[256,32]** window dimensions. The window analysis is conducted on a total of 9 scans from Scan 58 to Scan 66.

Statistical Analysis

The following analyses are done using [256,32] interrogation size window and 75% overlap. The data used to generate the following plots are from 38 scans, Scan 29 to Scan 66.

The border vectors of each scan was removed prior to any analysis as they were noticed to be highly inconsistent.

Velocity Convergence

The average horizontal velocity (across x & y) is observed to be increasing with time indicated as each scan is taken into account and is not converging.

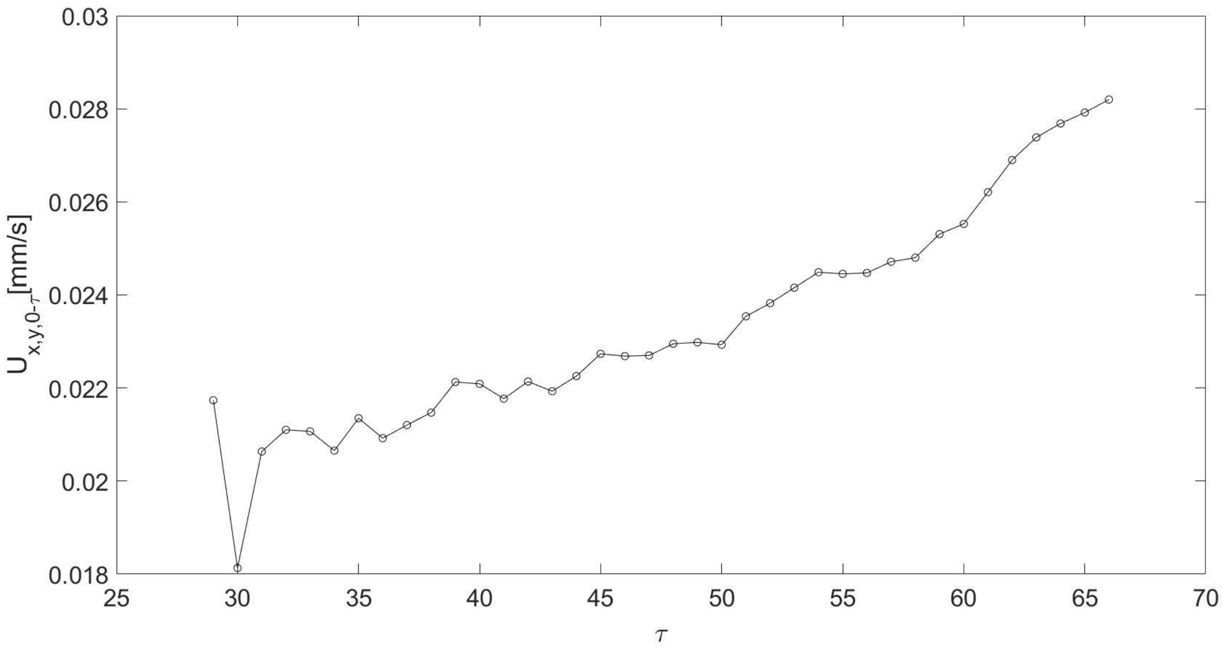

Figure 4: Convergence study of mean velocity averaged over the entire vector field and over an increasing number of scans 0 τ

Spatial Variation in Mean Velocity

The middle section, on average, displays higher horizontal velocity (averaged over all y-spanwise and all scans) compared to the sides of the scan. This graph will be paired with contour plots to look for any patterns in velocity with respect to bed-form elevations.

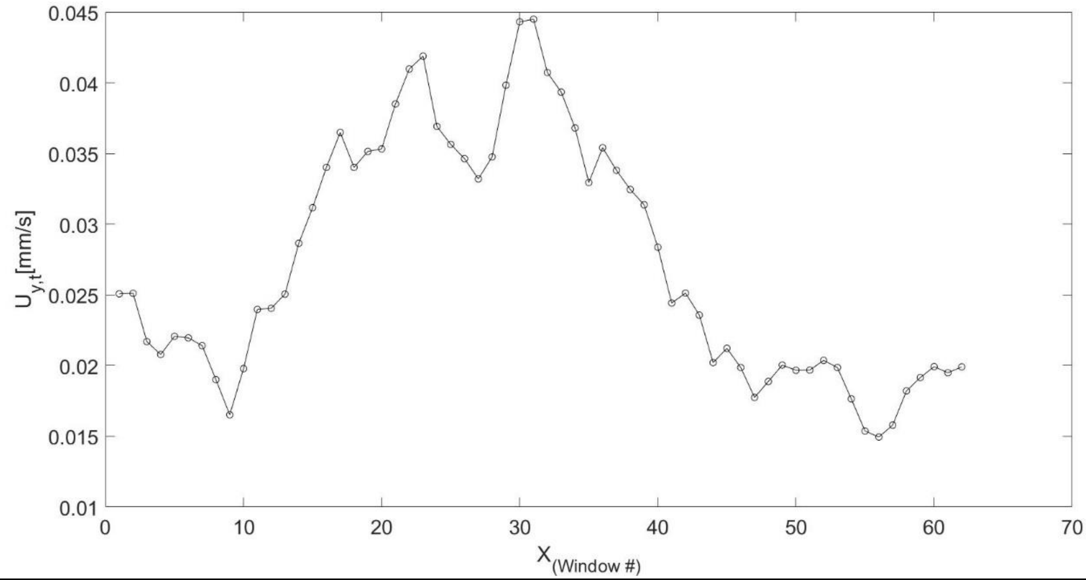

Figure 5: Study of mean velocity averaged over y,t and over x

Temporal Variation in Mean Velocity

The velocity averaged across the spatial dimensions seem to fluctuate with respect to time but overall display an inclination to increase, consistent with the velocity convergence plot.

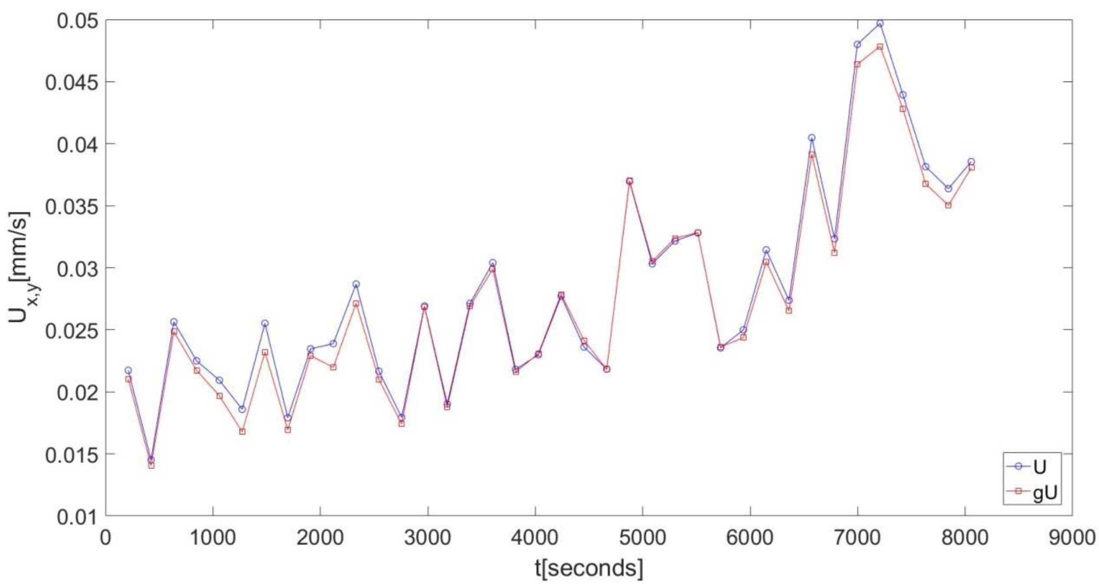

Figure 6: Study of mean velocity averaged over vector field against time, comparison between unfiltered and globally filtered data

PIV Overlap Analysis

The prior work is based on 75% overlap in PIV operations. The following demonstrates the difference between 50% (standard) and 75% overlap.

Velocity Convergence

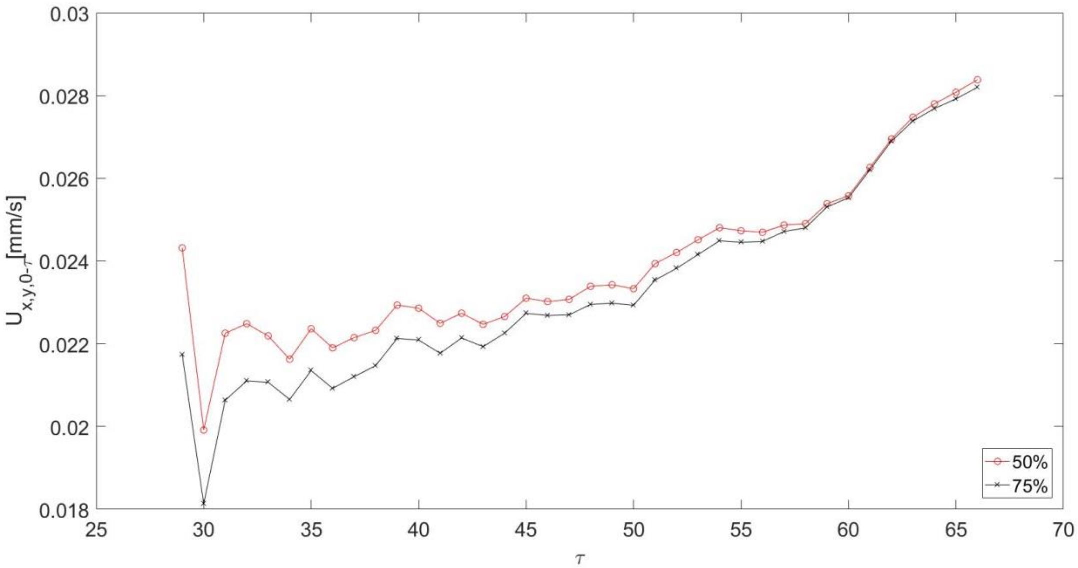

Figure 7: Convergence study of mean velocity averaged over the entire vector field and over an increasing number of scans 0- τ, with comparison between PIV overlap

Spatial Distribution of Averaged Velocity across y

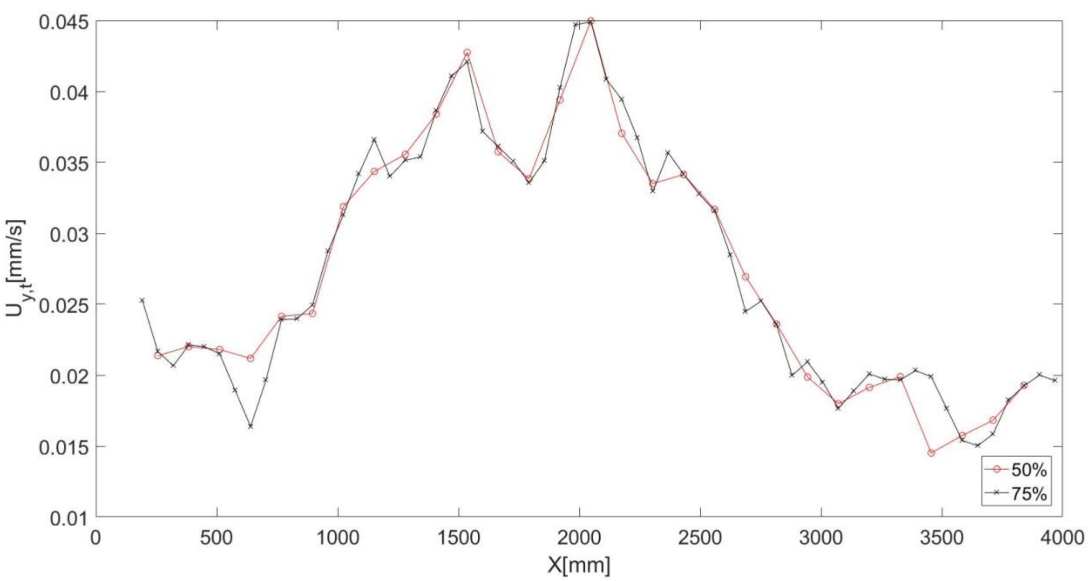

Figure 8: Study of mean velocity averaged over y,t and over x, with comparison between PIV overlap

Temporal Distribution of Velocity averaged across space

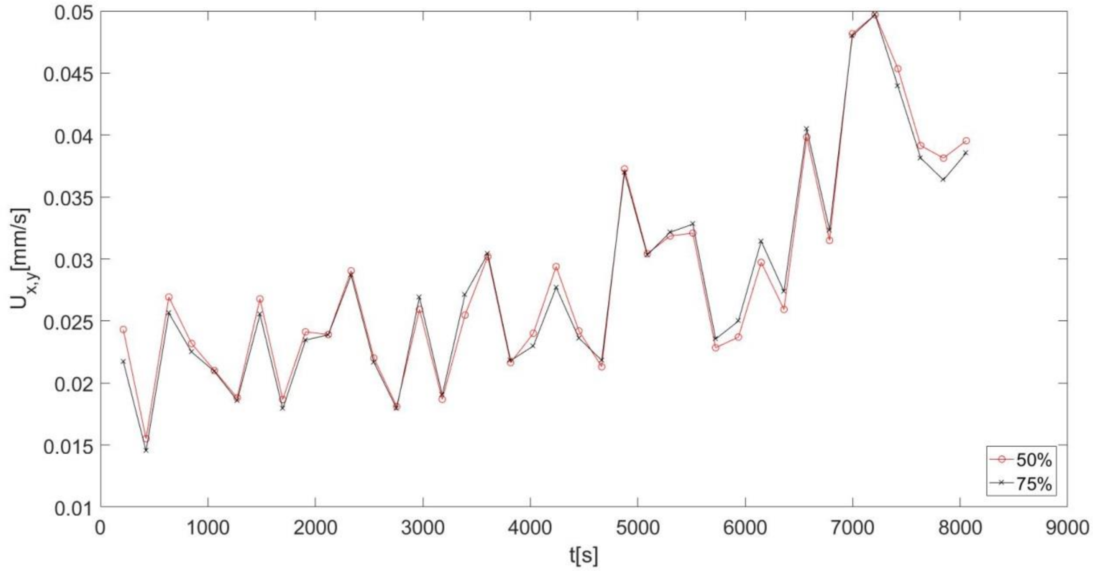

Figure 9: Study of mean velocity averaged over vector field against time, with comparison between PIV overlap

Horizontal Velocity RMS Plot

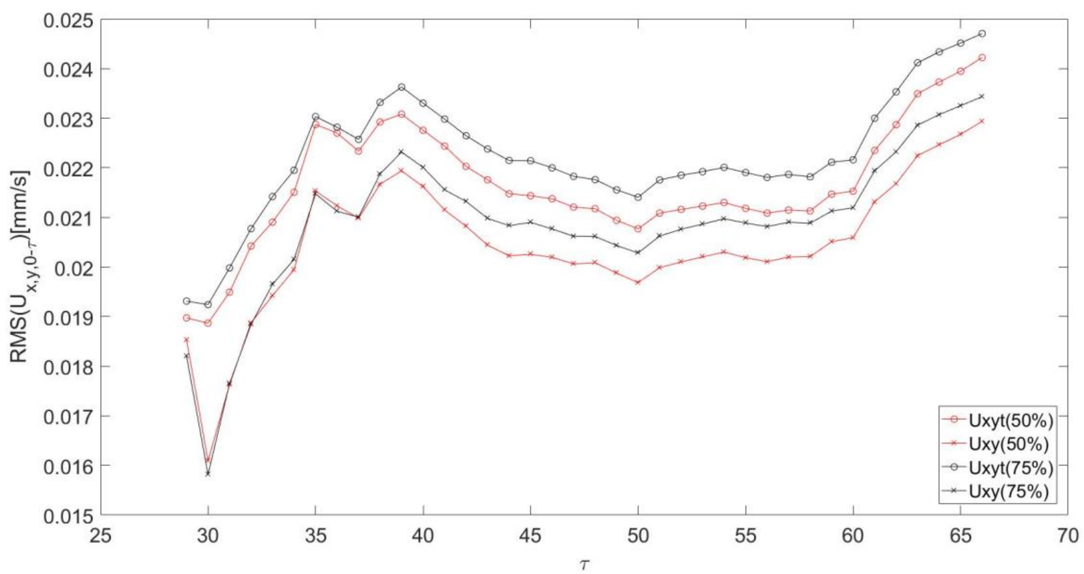

Figure 10: Comparison of convergence study of RMS velocity between PIV overlaps; t indicates fluctuations computed using a local average, not a global (one number) average

RESULTS

Spatial Auto-Correlation Analysis

Complete decorrelation of the signal (zero crossing) occurs around the 1000mm mark. Fluctuations based on local averages shows decreased lag. The auto-correlation sequence corresponds with the wavelength of the dunes, approximately 1 meter in length.

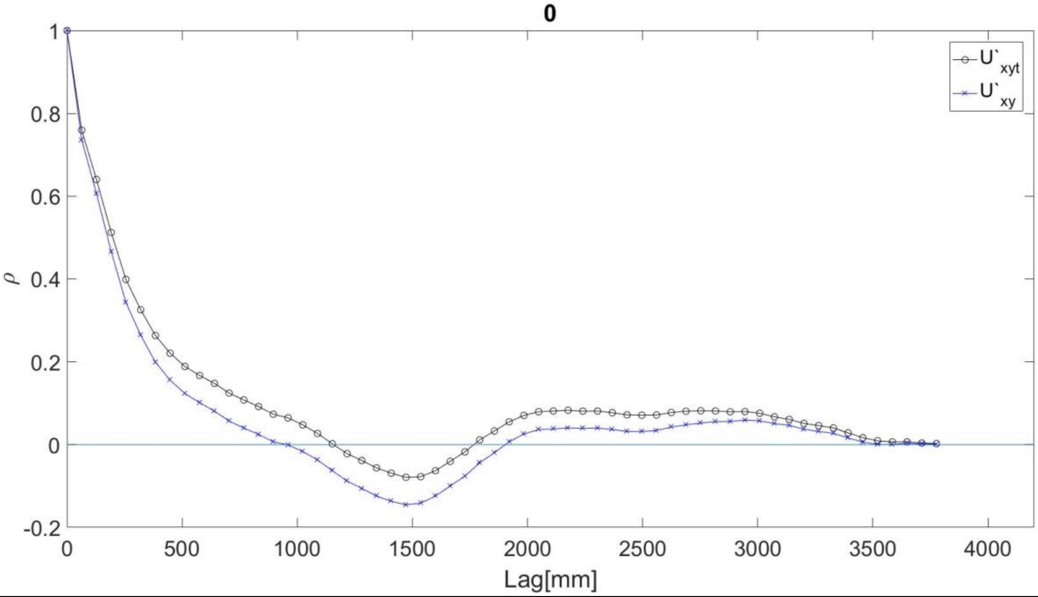

Figure 11: Spatial Auto-Correlation of Mean Velocity with comparison between fluctuations with global and local averages.

Temporal Auto-Correlation Analysis

In contrast to spatial auto-correlation, the sequence with global average incurs the zero crossing significantly before the other at around 100 minutes opposed to 130 minutes.
The decay on the sequence is also less drastic as compared to the spatial correlation sequence.

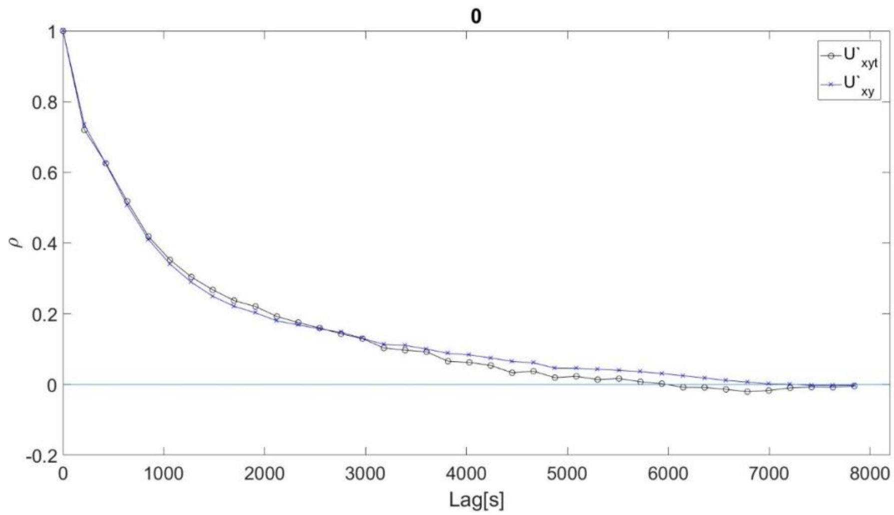

Figure 11: Temporal Auto-Correlation of Mean Velocity with comparison between fluctuations with global and local averages

Spatial Auto-Correlation

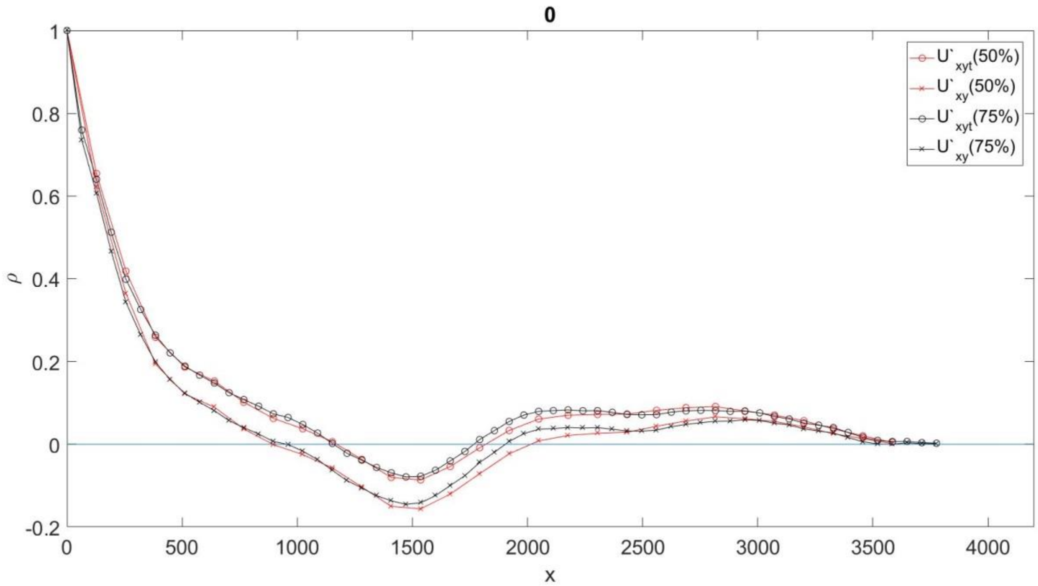

Figure 13: Spatial Auto-Correlation of Mean Velocity with comparison between fluctuations with global and local averages, and PIV overlap

Temporal Auto-Correlation

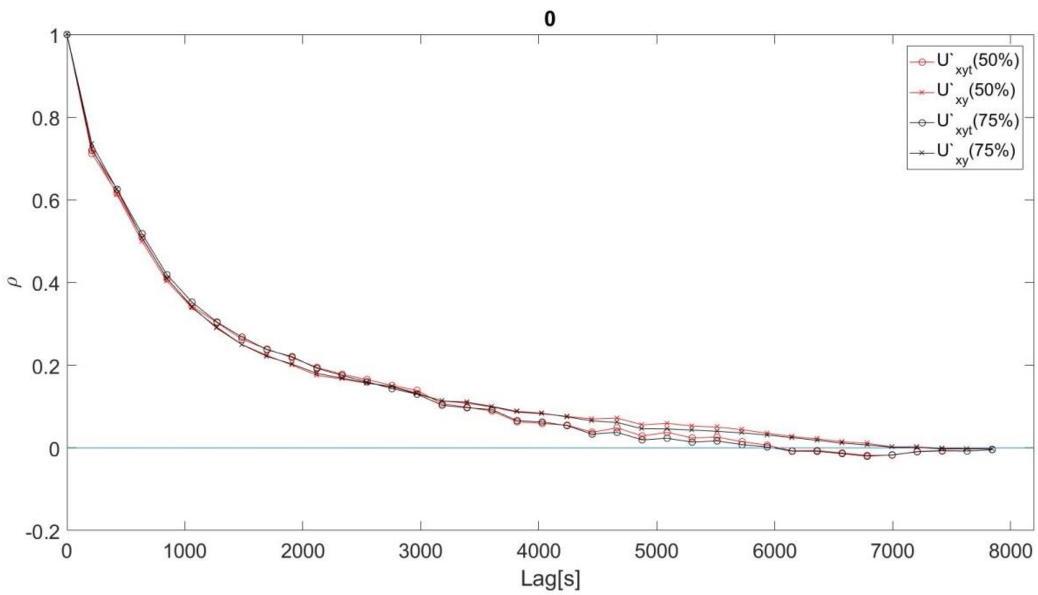

Figure 14: Temporal Auto-Correlation of Mean Velocity with comparison between fluctuations with global and local averages, and PIV overlap

PIV Delta t Analysis

In effort to support the reliability of PIV analysis, the procedure is executed on scans 1, 2 and 3 dt away to compare velocities. Two sample scan sets (40-43,54-57) is selected and velocity is computed. The results are tabulated:

Scan 40	$\overline{\boldsymbol{U}}$(mm/s)	$\overline{\boldsymbol{V}}$(mm/s)
1 dt	0.0334	4.677e-5
2 dt	0.0334	3.359e-5
3 dt	0.0328	1.299e-5
Scan 54	$\overline{\boldsymbol{U}}$(mm/s)	$\overline{\boldsymbol{V}}$(mm/s)
1 dt	0.0219	-3.416e-5
2 dt	0.0249	-2.711e-5
3 dt	0.0272	-3.261e-5

Table 4: Analysis of mean velocity based on comparison between time difference(dt) in PIV

Elevation-Velocity Analysis

The elevation of the centerline is extracted and its corresponding velocities are averaged across all scans(time) to produce average velocities with respect to the elevation. 97.35% of the available data is represented in the range that the brackets cover.

Six elevation brackets are defined as follows:

Brackets: (mm)
1 - (-30 to -20)
2 - (-20 to -10)
3 - (-10 to 0)
4 - (0 to 10)
5 - (10 to 20)
6 - (20 to 30)

The results are tabulated:

Bracket	$\overline{\boldsymbol{U}}$**(mm/s)**
1	0.0303
2	0.0286
3	0.0288
4	0.0268
5	0.0284
6	0.0311

Table 5: Mean horizontal velocity with respect to elevation bracket

The results above are calculated based on elevations matched with velocities at the center on the interrogation window. The following results are based on velocities matched with the averaged elevation across the span of the interrogation window [512,64] mm.

The results are tabulated:

Bracket	$\overline{U}$**(mm/s)**
1	0.0259
2	0.0305
3	0.0279
4	0.0267
5	0.0330
6	0.0359

Table 6: Mean horizontal velocity with respect to elevation bracket averaged across interrogation window

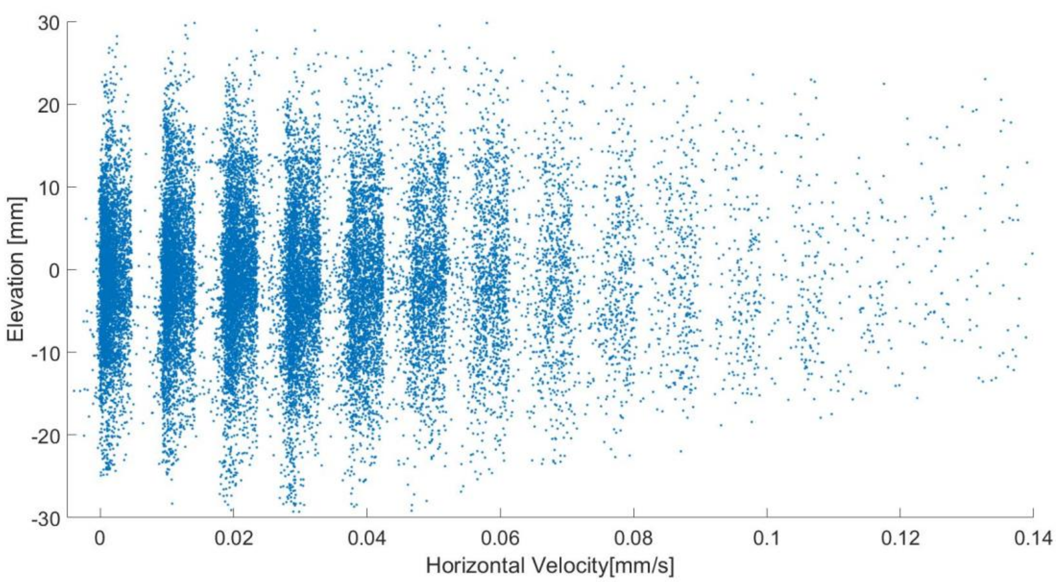

Figure 15: Distribution of velocity with respect to averaged elevation across interrogation window